# A COMPREHENSIVE STUDY ON THE MICROSTRUCTURE AND OPTICAL PROPERTIES OF $Fe_3O_4$ NANOPARTICLES BY VARIATION OF TEMPERATURE AND NaOH CONCENTRATION

**I Putu Tedy Indrayana[1]*, Sil Tunang[1], Yuli M Huragana[1], Nurul Imani Istiqomah[2], Edi Suharyadi[2]**

[1]*Physics Study Program, Faculty of Natural Science and Engineering Technology, Universitas Halmahera*
*Kompleks GMIH, St.Trans-Tobelo, Wari Ino Tobelo 97762, Halmahera Utara, Maluku Utara- INDONESIA*
[2]*Department of Physics, Faculty of Natural Science and Mathematics, Universitas Gadjah Mada*
*St. Bulaksumur, Sekip Utara, Sinduadi 55281, Sleman, Yogyakarta - INDONESIA*
*e-mail: tedyindrayana@gmail.com

## ABSTRACT

*This work was aimed at optimizing the microstructure and optical properties of $Fe_3O_4$ by variation of synthesis temperature and NaOH concentration. The nanoparticles have been synthesized from iron sand by using the coprecipitation method. The temperature was varied of 60°C, 80°C, and 100°C, while NaOH concentration was 3 molar, 5 molar, and 7 molars. The microstructural parameters were characterized by using X-ray Diffraction (XRD) and Scanning Electron Microscopy (SEM) techniques. The optical properties were characterized by using Fourier Transform Infrared Spectroscopy (FTIR) and UV-Vis Spectroscopy, consecutively. The results showed that the crystallite size of $Fe_3O_4$ increase with an increment of synthesis temperature due to higher thermal energy driving the nucleation process. The crystallite sizes were in the range of 3.77 nm – 20.37 nm. Increasing NaOH concentration also affected the increment in crystallite sizes. On the other hand, an excess of NaOH concentration influences the formation of smaller crystallite sizes of $Fe_3O_4$ with smaller crystal density and larger microstrain. The existence of $Fe^{2+}$-O and $Fe^{3+}$-O vibration in FTIR spectra confirmed the formation of $Fe_3O_4$ nanoparticles. The direct and indirect optical gap energies of $Fe_3O_4$ were in the range of 3.15 eV – 3.39 eV and 2.39 eV – 2.91eV. The synthesis temperature and NaOH concentration have a significant role in controlling the properties of $Fe_3O_4$.*

Keywords: *Microstructure; NaOH; Optical Properties; Synthesis Temperature*

## INTRODUCTION

Since a century, $Fe_3O_4$ has been studied by material researchers around the world. It has been a promising material due to its unique physical and chemical properties. Because of those properties, so the $Fe_3O_4$ has many potential applications, for instance in the case of the biosensor, the $Fe_3O_4$ nanoparticle has been used as promising matrices for immobilization of desired biomolecules (Ali, et al., 2013). Due to its catalytic properties, the $Fe_3O_4$ has been applied as electrocatalytic material for the nitrite sensor (Qu, et al., 2015). In case of biomedical field, the $Fe_3O_4$ can be used as contrast agent materials for magnetic resonance imaging (MRI), magnetic carrier for targeting drug delivery system, and heat generator in magnetic hyperthermia system (Ghazanfari, et al., 2016; Revia & Zhang, 2016), target-specific cell internalization carrier for chemotherapy (Mohammad, et al., 2017). In the field of environmental protection, the $Fe_3O_4$ with its modification has been applied as removal agent of petroleum oil from contaminated waters and soil (Murgueitio, et al., 2018) and as an adsorbent for heavy metal removal (Anush & Vishalakshi, 2019).

The properties performed by the $Fe_3O_4$ strongly affected by its crystal structure and microstructure. The $Fe_3O_4$ has an inverse spinel structure within a face-centered cubic (FCC) cell in the cubic crystal system and space group of $Fd\bar{3}m$ (Fig.1). The unit cell contains 96 sublattices occupied by 24 cations, 8 of them distribute in 64 tetrahedral sublattices and the remaining 16 cations distributed in 32 octahedral sublattices. Simultaneously, cation distribution formula of the $Fe_3O_4$ is $(Fe^{3+})[Fe^{2+}Fe^{3+}]O_4^{2-}$, where cation $Fe^{2+}$ fully occupies octahedral sublattices and $Fe^{3+}$ is distributed both in tetrahedral and octahedral sublattices (Mathew & Juang, 2007; Ghazanfari, et al., 2016; Reddy & Yun, 2016).

The microstructure of the $Fe_3O_4$ involves lattice parameter of the unit crystal ($a$), microstrain ($\varepsilon$), crystal density ($\rho_x$), crystal dislocation density ($\delta$), and crystallite size ($t$). Those parameters are directly affected by the synthesis of the $Fe_3O_4$ nanoparticles. There are three methods have been

carried out for synthesizing $Fe_3O_4$, such as chemical, physical, and biological method. The chemical method involves sol-gel, microemulsion, hydrothermal, electrochemical decomposition, sonochemical, thermal decomposition, and coprecipitation. The physical method involves gas-phase aerosol, electron beam lithography, pulsed laser ablation, laser-induced pyrolysis, power ball milling, and aerosol. The last, biological method involves plan mediated, fungi mediated, bacteria mediated, and protein-mediated (Ali, et al., 2016). Among those methods, chemical coprecipitation is considered very appropriate method for synthesizing the $Fe_3O_4$ nanoparticles due to its simple procedure, short reaction time, high yield, low synthesis temperature (20°C – 150°C), relatively narrow size distribution, and cost-effective (Ramadan, et al., 2011; Ali, et al., 2016; Ghazanfari, et al., 2016; Hameed, et al., 2017).

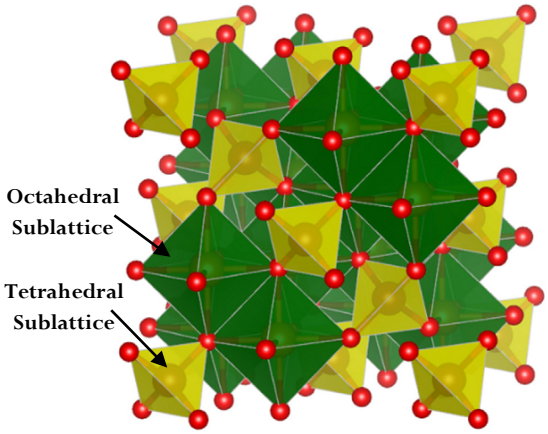


**Figure 1**. Model of the $Fe_3O_4$ crystal structure (Reddy & Yun, 2016)

In this study, we reported the effect of synthesis temperature and NaOH concentration on the microstructure and optical properties of the $Fe_3O_4$ nanoparticles. Both synthesis temperature and NaOH concentration are the dynamical factors that strongly influence the nucleation rate and growth rate of the $Fe_3O_4$ crystal seed. The microstructure and optical properties of the $Fe_3O_4$ nanoparticles are very sensitive to those factors. Many research (Ramadan, et al., 2011; Yusoff, et al., 2017; Salviano, et al., 2018; Hu, et al., 2019) have been explored about the effect of synthesis temperature and the pH correlated with base concentration on the physical properties of the $Fe_3O_4$, but only a few papers reported their comprehensive study in case of the detail explanation for physicochemical point of view. In this works, we also reported the synthesis of $Fe_3O_4$ nanoparticles from local iron sand which has an advantage for the use of local mineral deposited in Halmahera Utara to be advanced nanomaterials. In a brief, the crystallite size of the $Fe_3O_4$ nanoparticle increase with increasing both synthesis temperature and NaOH concentration. The $Fe_3O_4$ has been proved to be semiconductor materials due to the low optical bandgap. Therefore, $Fe_3O_4$ can be a good candidate for photonic materials.

## MATERIALS AND METHODS

### Raw Materials and Precursor

Local iron sand of Wari Ino beach has been used for providing Fe cation. Hydrochloric acid (HCl) 37% (Sigma-Aldrich) was used as a solvent for Fe extraction from iron sand. The precipitating agent was NaOH (Merck Emsure) purchased from LPPT UGM Yogyakarta.

### Preparation of Iron Sand

Iron sand of 120 grams was taken by using a permanent magnet. The iron sand was separated carefully from the impurities and washed three times by using distilled water. The iron sand was heated up in an oven at a temperature of 50°C for 1 hour until they are dry. For synthesizing one sample, the dried iron sand of 20 grams then extracted by using 20 ml HCl (37%). The extraction was carried out by stirring up the iron sand at room temperature for about 10 minutes to obtain Fe solution. After stirring, the resulted solution will be yellowness brown in color. These solutes were filtered from the sand and ready to use for synthesizing $Fe_3O_4$ nanoparticles.

### Synthesis of the $Fe_3O_4$

First of all, the Fe solution of 20 ml was heated up at a constant temperature of 50°C for 30 minutes to activate the Fe cation in the solution, and then the temperature was dropped down naturally until it reached thermal equilibrium with the room. The NaOH solutions of 3M, 5M, and 7 M were prepared as the precipitating agent. The temperature of NaOH solutions was kept at constant values of 60°C, 80°C, and 100°C. The synthesis temperature used for NaOH concentration variation was 80°C, while the NaOH concentration used for synthesis temperature variation was 3M.

The Fe solution was started to drop wisely to the NaOH solution when the temperature reaches to those values. This synthesis process was conducted for 60 minutes. After the synthesis, black slurry on the bottom of the glass will be obtained. This slurry is magnetically in nature. Therefore, the glass was placed on the permanent magnet to drive the separation process between slurry and the water. The slurry was separated into the water and

then rinsed by distilled water four times. The slurry was heated up at a constant temperature of 100°C for 4 hours to obtain dry chips. The chips were grounded by using mortar and pestle to obtain a tiny black powder of $Fe_3O_4$. This powder was continued to calcination at a constant temperature of 250°C for 4 hours.

### Characterization Methods and Instruments

The samples of $Fe_3O_4$ nanoparticles were characterized for their crystal structure and microstructure by using X-ray Diffraction-XRD (Merk PanAnalytical-Expert Pro) over the $2\theta$ scan range of $10^o - 90^o$ at a scan step of $0.002^o$ and using Cu-Kα radiation with a wavelength of 1.540598Å. The surface morphology and elemental composition of the $Fe_3O_4$ nanoparticles were characterized by using Scanning Electron Microscopy-SEM (Merck Merk FEI- Inspect-S50) coupled by Electron Diffraction Spectroscopy-EDS.

The vibrational spectra of functional group bonds were characterized by using Fourier Transform Infrared Spectroscopy-FTIR (Merk Paragon 1000PC Perkin Elmer) over the wavenumber range of 400 $cm^{-1}$ – 4000 $cm^{-1}$. The absorbance spectrum of samples was characterized by using Specular Reflection UV-Visible Spectroscopy-UV-Vis SR (Merk Pharmaspec UV-1700) over a wavelength range of 200 nm – 800 nm.

## RESULTS AND DISCUSSIONS

### Crystal Structure and Microstructural Parameters

Information about crystal structure and microstructural parameters of the sample can be obtained from the XRD pattern. First of all, herewith is displayed the XRD pattern of raw iron sand by Figure 2. There were four phases investigated in the raw iron sand, i.e., $\alpha$-$Fe_2O_3$ (JCPDS No 33-0664-Rhombohedral), $\varepsilon$-$Fe_2O_3$ (JCPDS No 16-0653-Monoclinic), $Fe_3O_4$ (JCPDS No 11-0614-Cubic spinel), and γ-$Fe_2O_3$ (JCPDS No 13-0458-Tetragonal). The highest intensity of the diffraction peak belongs to the $Fe_3O_4$ phase of the diffraction plane (311). The phase of $Fe_3O_4$ is predominantly composed of raw iron sand. Other phases might be formed as a result of the oxidation process experienced by $Fe_3O_4$ since years ago. Different kind of oxidation state of the $Fe_3O_4$ is mainly caused by environmental factors, such as temperature, pressure, climate, and the existence of oxygen molecules in the air.

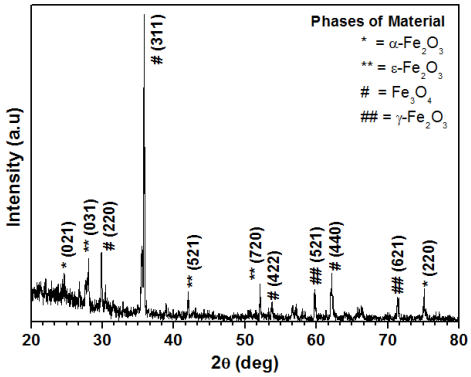


**Figure 2**. XRD pattern of raw iron sand sample

The synthesized $Fe_3O_4$ nanoparticles have different XRD patterns such displayed in Fig. 3 and Fig. 4. The raw XRD pattern of $Fe_3O_4$ by NaOH concentration variation can be displayed by Fig. 3. The XRD patterns confirm the formation of polycrystalline nanoparticles $Fe_3O_4$. There are five main diffraction peaks observed, such as (220), (311), (400), (511), and (440). The XRD patterns seem full of noise which means that the samples have a low crystalline state. The broadening peak of XRD indicates that ultrafine particles have been formed. The highest intensity of the diffraction peak was found owing by (311). It refers that the $Fe_3O_4$ nucleus tends to grow in [311] direction compared to others. This is a characteristic of $Fe_3O_4$ where the easy direction for the nucleation is in [311] such figured out in JCPDS no 11-0614.

The diffraction peaks of $Fe_3O_4$ samples are relatively broad. In the case of NaOH concentration variation, the diffraction peaks become broader as increasing concentration. For instance, the diffraction peaks of (220), (400), and (511) for sample $Fe_3O_4$ NaOH 3M seem clear, but they become broader and relatively many noises in the sample of NaOH concentration 7M. Somehow, the peak's intensity also decreases with increasing NaOH concentration.

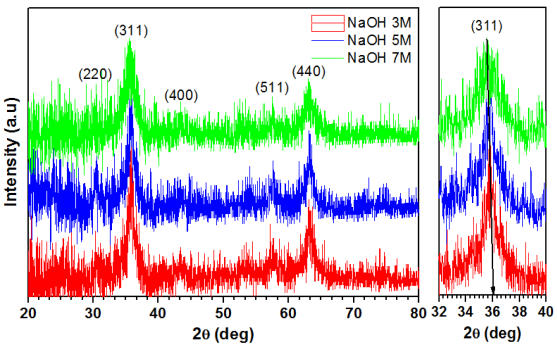


**Figure 3**. XRD pattern of samples with NaOH concentration variation.

NaOH in the coprecipitation process has a significant role in providing $OH^-$ anion for the formation of an iron hydroxide compound. As reported by (Mascolo, et al., 2013) the chemical reaction (1) for the coprecipitation is

$$2FeCl_3 + FeCl_2 + 8NaOH \quad Fe_3O_4 + 4H_2O + 8NaCl \,. \quad (1)$$

This reaction explicitly shows that the formation of $Fe_3O_4$ is started by the formation of ferric hydroxide and ferro hydroxide compound, such as reaction (2),

$$2Fe(OH)_3 + Fe(OH)_2 \quad Fe_3O_4 + 4H_2O \,. \quad (2)$$

According to reaction (2), larger NaOH concentration causes an increase in reaction rate for the formation of the hydroxide compound. Therefore, the rate for the nucleation process is also increased due to higher thermal energy produced by the collision between particles that tend to aggregate in a larger size due to their magnetic properties in nature. Technically, the NaOH concentration directly controls the pH of the medium for nucleation. As the reaction rate for nucleation becomes higher then a bigger crystallite size of $Fe_3O_4$ will be produced, as provided in Table 1. The crystallite size of $Fe_3O_4$ samples was calculated by using Scherer's formula as explained by (Ghandoor, et al., 2012). The crystallite size of the $Fe_3O_4$ nanoparticle increases by increasing NaOH concentration up to 5M and then decreases as NaOH concentration increase up to 7M. This result is in agreement with the phenomenon reported by (Raz, et al., 2012). 5M becomes a critical concentration of NaOH for this coprecipitation. At a lower critical value, the particles keep in growing even after their formation. Larger particles are more energetically stable compared to smaller particles in the reaction. If the NaOH concentration is larger than the critical value, so the crystallite size of the $Fe_3O_4$ becomes smaller. This phenomenon can be explained based on excess $OH^-$ anion. If the concentration of $OH^-$ anion is much larger than that $Fe^{2+}$ and $Fe^{3+}$, so over-saturation will occur during the coprecipitation process and promoting the formation of smaller crystallite size as explained by (Mascolo, et al., 2013).

Increasing the NaOH concentration also influences the diffraction peaks position, the main peak of (311). There is a shift of peak (311) to a lower diffraction angle $2\theta$ as NaOH concentration increases. This phenomenon refers to the expansion that occurs on the unit cell of the crystal $Fe_3O_4$. Increasing NaOH concentration up to critical value influences an increase of the nucleation growth and expansion of the unit cell. This is proved by an increase in the lattice parameter of the $Fe_3O_4$. The obtained values of the lattice parameter, in this case, are lower than the reference values given in JCPDS No 11-0614, but they are close to the value reported by (Ghandoor, et al., 2012).

The defect in the unit cell of the $Fe_3O_4$ has been observed due to rapid nucleation growth that is caused by an increase of NaOH concentration. Quantitatively, the defect in a unit cell can be determined based on the value of microstrain $\varepsilon$. The highest defect occurs when the NaOH concentration 7M for which over-saturation occurs and the nucleation process becomes unstable. The defect in the unit cell decrease when the NaOH concentration increases up to 5M. Physically, the defect in the unit cell can cause by a displacement of atoms in the entire unit cell. The displacement of atoms makes the distance between atoms far away from each other. Therefore, the interstitial space between atoms becomes larger and that causes a decrease in crystal density ($\rho_x$) of the $Fe_3O_4$ nanoparticles, as explained by (Siregar, et al., 2017). The values of crystal x-ray density of $Fe_3O_4$ samples are larger than that given by JCPDS No 11-0614.

Synthesis temperature also has a significant role in determining the microstructure of nanoparticles. Some researches reported by (Faraji, et al., 2010; Mascolo, et al., 2013; Tai, et al., 2014; Siregar, et al., 2017; Salviano, et al., 2018; Hu, et al., 2019) explain that there is a direct consequence between increasing synthesis temperature and improving the microstructure of nanoparticles. The XRD pattern of $Fe_3O_4$ due to synthesis temperature variation can be displayed by Fig. 4.

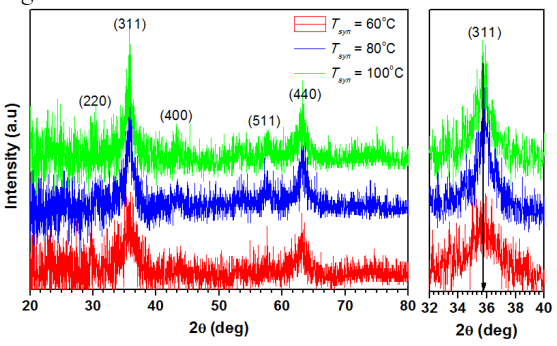


**Figure 4**. XRD pattern of samples with synthesis temperature variation.

The diffraction peaks profile shown by Fig. 4 is sharp and narrower as an increasing synthesis temperature. It refers to the formation of more crystalline nanoparticles as synthesis temperature increases. Synthesis temperature takes the role in

energizing the coprecipitation process by mean of thermal energy. Increasing the synthesis temperature means increasing thermal energy given to drive the reaction. The reaction rate will increase rapidly as the temperature increase. Note that, here the synthesis was conducted by using NaOH concentration of 3M at which is lower concentration than the critical value as explained before. Increasing synthesis temperature also provides a higher intensity of the diffraction peaks, for instance, peaks of (220), (400), and (511). In the case of diffraction angle, increasing synthesis temperature causes a shift of diffraction angle $2\theta$ to a larger value. This indicates a change in unit cell size occurs.

According to Table 1, the crystallite size of nanoparticles dramatically increases from 3.77 nm to 20.37 nm as the synthesis temperature increases from 60°C – 100°C. This phenomenon can be explained by two reasons. First, increasing synthesis temperature will activate a number of Fe cations in the precursor solution. The presence of more Fe cation will drive the formation of more energetically $Fe_3O_4$ nuclei so that the nucleation becomes stable and the particles become larger. In a lower synthesis temperature, only small thermal energy can activate the Fe cation. Therefore, excess of $OH^-$ anion will produce small crystallite size, as explained before. Second, increasing synthesis temperature will increase the mobility of cation and anion to react during the reaction, further increasing the frequency of collision between cation and anion. Therefore, the growth kinetic of $Fe_3O_4$ nanoparticles increases and a larger crystallite size will be produced (Mascolo, et al., 2013).

**Table 1**. Microstructural parameters of the $Fe_3O_4$

| Parameter | 3M/60°C | 3M/80°C | 3M/100°C | 5M/80°C | 7M/80°C |
|---|---|---|---|---|---|
| $t$ (nm) | 3.77 | 5.59 | 20.37 | 6.51 | 4.29 |
| $a$ (Å) | 8.324 | 8.312 | 8.310 | 8.322 | 8.343 |
| $\varepsilon$ (line/m) | 9.086 | 6.128 | 1.683 | 5.265 | 7.995 |
| $\rho_x$ (gram/cm$^3$) | 5.342 | 5.367 | 5.370 | 5.347 | 5.306 |

A change in unit cell size can be justified according to a change of the lattice parameter of crystal $Fe_3O_4$. Lattice parameter becomes shorter which indicates that the position of atoms becomes closer. Consequently, the bond length of atoms becomes shorter and the binding energy becomes larger. This condition has a direct effect on the microstrain and crystal density of $Fe_3O_4$.

Due to more crystalline nanoparticles are produced by higher synthesis temperature then the microstrain of the unit cell becomes smaller, as provided in Table 1. This finding indicates that smaller defect occurs in a unit cell of $Fe_3O_4$. Increasing synthesis temperature has been proved able to improve the crystallinity of the sample.

It is evident that if the unit cell of the crystal becomes denser by atoms, the crystal density of the unit cell becomes larger directly. This finding has been proved that increasing synthesis temperature can increase the crystal density of $Fe_3O_4$. These values are much larger than those reported by JCPDS No 11-0614.

## Surface Morphology and Elemental Composition

The morphology of grains nanoparticles is displayed in Fig. 5. Geometrically, the grain of $Fe_3O_4$ has an irregular shape. The size is also not uniform. There is a broad size distribution according to the SEM micrograph. This finding justifies that not perfect nucleation occurs during the synthesis process. This micrograph also informs that the formation of the amorphous phase in the sample which is in agreement with the existence of many noises in the XRD pattern, as displayed by Fig. 3 and Fig 4.

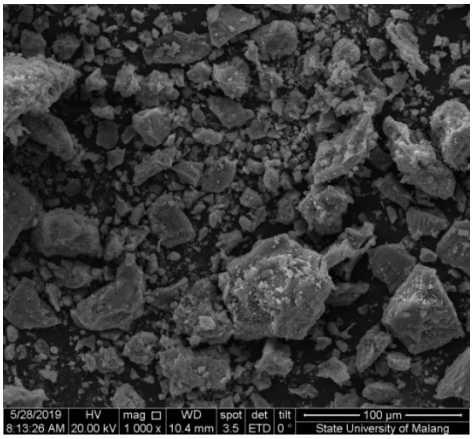


**Figure 5**. Surface morphology of $Fe_3O_4$ synthesized with 3M NaOH at a temperature of 80°C.

The elemental composition of sample nanoparticle $Fe_3O_4$ synthesized with 3M NaOH at a temperature of 80°C can be obtained from electron

diffraction spectra as displayed by Fig.6. According to the spectra, sample $Fe_3O_4$ is predominantly composed of Fe and O elements. Quantitatively, there are 53.26 wt% and 27 wt% composition of Fe and O elements, consecutively. Other elements have a much smaller composition compare to Fe and O. Other elements might be in the form of a free element that causes noise in the XRD pattern of $Fe_3O_4$ samples.

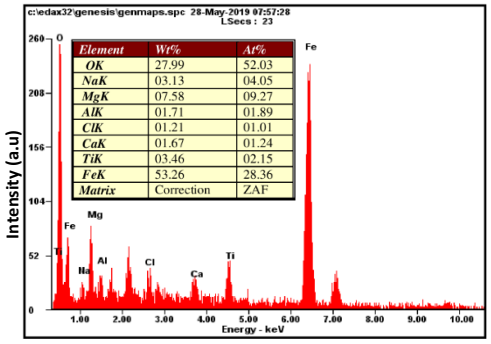


**Figure 6**. EDS spectra and elemental composition at the surface of $Fe_3O_4$ synthesized with 3M NaOH at a temperature of 80°C.

## Vibrational Spectra and Functional Group Bonds

The results of FTIR characterization are vibrational spectra such displayed by Fig. 7.

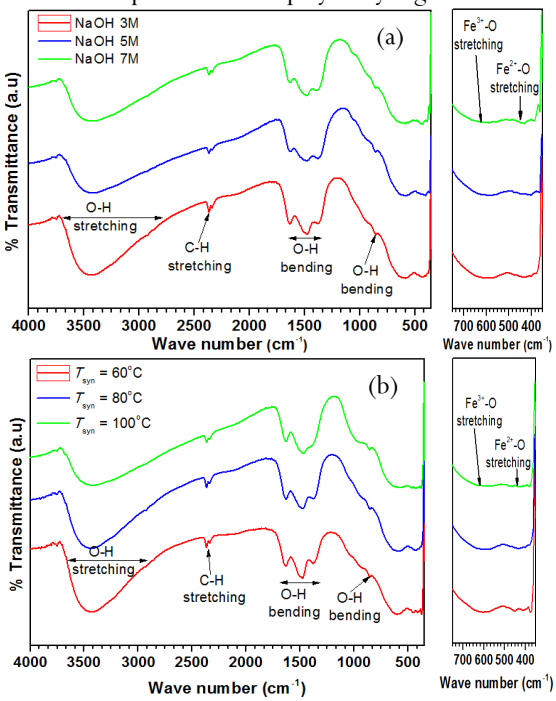


**Figure 7**. FTIR spectra of samples $Fe_3O_4$ with variation of: (a) NaOH concentration; (b) synthesis temperature.

According to the vibrational spectra, both groups of samples with NaOH concentration and synthesis temperature variation show the vibration of some functional group bonds. Two characteristic bonds, such as $Fe^{2+}$-O stretching and $Fe^{3+}$-O stretching have been successfully observed at a frequency range of 426.70 $cm^{-1}$ – 434.07 $cm^{-1}$ and 608.70 $cm^{-1}$ – 628.17 $cm^{-1}$, consecutively. These findings are in agreement with the result reported by (Saranya, et al., 2015; Takai, et al., 2019). The existence of these two vibrations implies that the formation of $Fe_3O_4$ phase with a cubic spinel crystal structure. The vibration of $Fe^{2+}$-O occurs in the octahedral sublattice, while $Fe^{3+}$-O occurs in the tetrahedral sublattice. A strong absorption occurs in the vibration spectra within this range of vibrational frequency indicates that the formation of a large number Fe-O vibration system. This evidence supports the results of both the XRD pattern and EDX spectra.

The vibration band at a frequency range of 856.88 $cm^{-1}$ – 863.19 $cm^{-1}$ is assigned to O-H bending vibration (Lopez, et al., 2010). This vibration also occurs at a frequency range of 1379.31 $cm^{-1}$ – 2377.51 $cm^{-1}$ (Lopez, et al., 2010; Saranya, et al., 2015).

Stretching vibration of O-H bond also occurs at a frequency range of 3442.38 $cm^{-1}$ - 3458.30 $cm^{-1}$ (Rahman, et al., 2012; Saranya, et al., 2015; Takai, et al., 2019). The vibrational energy of O-H stretching is higher than O-H bending due to higher vibrational frequency. The existence of those vibrations implies that the existence of water molecules on the surface of nanoparticles. The surface of $Fe_3O_4$ is hygroscopic in nature so that the $Fe_3O_4$ very reactive and easy to be oxidized by free oxygen ion. Somehow, the O-H group also is given by KBr materials used as a template for pellet preparation. This material is hygroscopic in nature so that it is very easy to react with O-H molecule in the air during preparation. The last, C-H stretching vibration is found exist in samples in a frequency range of 2337 $cm^{-1}$ - 2400 $cm^{-1}$ as a result of interaction between $Fe_3O_4$ and $CO_2$ and $H_2$ molecules in the air.

The effect of NaOH concentration and synthesis temperature is mainly on the specific vibrational frequency owned by each functional group bond. First, according to index figures (see Fig.7), there is a shift of vibrational frequency to a larger value due to an increase of NaOH concentration and synthesis temperature. This indicates that the vibrational energy of the bond becomes larger due to a closed position of atoms both Fe and O within the unit cell. Second, increasing NaOH concentration and synthesis temperature causes a reduction of O-H group bond

volume which indicates that more crystalline samples have been produced. In the hand, the volume of Fe-O bond becomes larger that is proved by a larger deep area of Fe-O band within the FTIR spectra.

**Absorbance Spectra and Optical Properties**

Optical characterization of samples $Fe_3O_4$ provides absorbance spectra such as displayed by Fig. 8. The absorbance spectra of samples were measured in a wavelength range of 200 nm – 800 nm. The absorbance spectra of $Fe_3O_4$ both due to NaOH concentration and synthesis temperature variation are broad. It is caused by large particle size distribution as confirmed by SEM micrograph, different particle size morphology, and impurities attached to the surface of $Fe_3O_4$. Moreover, wideband absorbance spectra are also caused by a defect in the crystal of $Fe_3O_4$.

The intensity of the absorbance refers to the number of photon energy absorbed by nanoparticles at a specific wavelength. According to Fig. 8a., a sample of 5M NaOH/80°C has the highest absorbance and a sample of 3M NaOH/80°C has the lowest absorbance for NaOH concentration variation. On the other hand, the sample of 3M NaOH/60°C has the highest absorbance and a sample of 3M NaOH/80°C has the lowest absorbance for synthesis temperature variation. Optically, a sample with lower absorbance is more transparent then sample with higher absorbance.

Graphically, the maximum peak of each spectrum varies. In the case of NaOH concentration variation, the absorbance spectra tend to experience redshifting. The maximum absorbance peak for each spectrum tends to shift to a larger photon wavelength. This means smaller photon energy needed by electron to excite from lower energy state to higher energy state. In contrast, samples with synthesis temperature variation tend to experience blue shifting. This implies that higher photon energy needed by electron to excite from lower energy state to higher energy state when then synthesis temperature of the nanoparticle increase.

Another profile of the absorbance spectra is cut-off wavelength ($\lambda_{cut\text{-}off}$). When the absorbance peak goes down after the maximum point so the value will drop down linearly as increasing photon wavelength in a range of 300 nm – 400 nm. Therefore the value $\lambda_{cut\text{-}off}$ will different depend on the absorbance spectra profile. A larger value of $\lambda_{cut\text{-}off}$ implies a smaller gap occurs between the valence band and conduction band of the nanoparticle. In regard to the NaOH concentration variation, the $\lambda_{cut\text{-}off}$ shifts to a higher value with increasing the NaOH concentration. It means that smaller distances between the valence band and conduction band within the electronic structure of $Fe_3O_4$ nanoparticles.

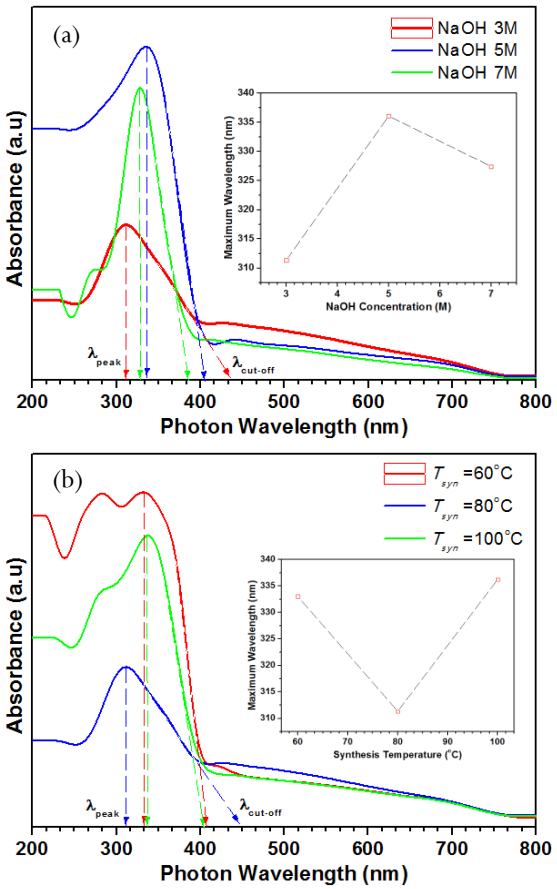


**Figure 8**. Absorbance spectra of $Fe_3O_4$ with variation of: (a) NaOH concentration and (b) synthesis temperature variation.

In relation to the bandgap of the $Fe_3O_4$ nanoparticles, in this research, we also provide detail values of their optical bandgap. The optical band gap of nanoparticles can be classified into two groups, such as the direct bandgap and indirect bandgap. If the interband transition of an electron occurs between the highest peak in the valence band to the corresponds the lowest valley in the conduction band with same momentum *k*, then the energy needed by electron to directly across the bandgap, leaving a hole in the valence band refers to direct optical gap energy (see Fig. 9a). In other hand, if the interband transition occurs at which the peak of the valence band doesn't correspond to the lowest point of the conduction band (increment of momentum *k*) so the total energy needed by electron to interact with both photon and a phonon simultaneously to jump the gap refers to the indirect bandgap (see Fig.9b) (Tiley, 2011).

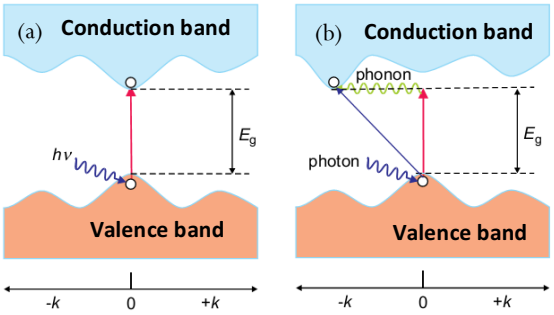


**Figure 9**. Optical gap energy structure: (a) direct band gap and (b) indirect band gap (Tiley, 2011).

Both direct and indirect optical gap energy can be calculated by using Tauch's plot equation (3): (Mote, et al., 2015; Anjum, et al., 2018)

$$(\alpha h\nu)^n = A(h\nu - Eg), \quad (3)$$

where $h\nu$ is the photon energy (eV), $\alpha$ is the absorption coefficient ($cm^{-1}$), $A$ is a constant which depends on the transition probability, and $n$ is an index which characterize the optical transition process. The value of $n = 2$ for allowed indirect interband transition process and $n = 1/2$ for allowed direct interband transition process. Hence, the absorption coefficient is calculated by using equation (4) (Anjum, et al., 2018):

$$\alpha = 2.303 \cdot \frac{Abs}{t_p} \quad (4)$$

where $Abs$ is the normalized absorbance and $t_p$ is the thickness of pellet. In this research, measured sample of $Fe_3O_4$ nanoparticles is in form of pellet with thickness of 1 mm.

Both direct and indirect band gap energy are determined by extrapolation the linear portion of curve between $(\alpha h\nu)^n$ and photon energy $h\nu$ until $(\alpha h\nu)^n = 0$. Therefore, the cut-off photon energy given by this method is the optical gap energy of the nanoparticles. In the case of the variation NaOH concentration, the direct and indirect optical gap energies can be displayed in Fig. 10.

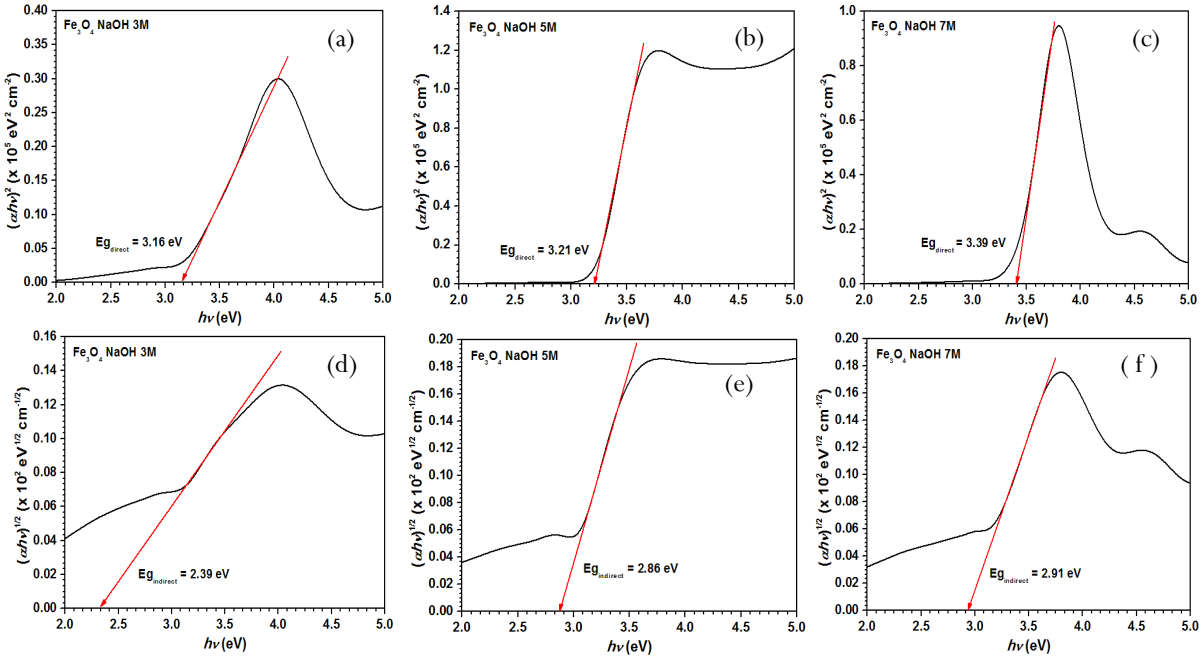


**Figure 10**. Tauch's plot of direct (a – c) and indirect (d – f) optical gap energies for NaOH concentration variation.

According to Fig. 10, the values of the direct optical gap energy of the $Fe_3O_4$ nanoparticles are increasing with increasing NaOH concentration. This result is contradictive compared to the result reported by (Dhas, et al., 2015; Heiba, et al., 2015; Loganathan & Kumar, 2016). The indirect optical gap energy also increases with increasing NaOH concentration. Ideally, as a consequence of a quantum confinement effect, the optical band gap energy decreases with increasing particle size. The optical gap energy is strongly correlated to the size of particles. Unfortunately, the fact is that in these findings, both crystallite size and the optical gap energy have the same trend. The optical gap energy increases with an increase of crystallite size. This is a novel phenomenon we have been observed ever. There are some reasons we can propose to explain this phenomenon. First, a change in NaOH concentration might changes the cation distribution of $Fe^{3+}$ and $Fe^{2+}$ within the unit cell in tetrahedral and octahedral sublattice. This condition will influence a change in the electronic band structure

of the nanoparticles. Increasing NaOH concentration tends to enlarge the interband space of the nanoparticle and so the electronic structure will change. If the interband space becomes larger so larger optical gap energy will be produced. Second, increasing NaOH concentration allows the expansion of the unit cell of the $Fe_3O_4$ which is proved by an increase of lattice parameter. This indicates that a change of the atomic position which allows a change in the atomic bond length. This reason is supported by evidence that the microstrain of the nanoparticles increases as the NaOH concentration increase. Of course, the defect occurs significantly within the crystal structure and it possible to cause a change in the crystal symmetry and the interband transition of the electron (Scott , 2007). Third, in case of the size of nanoparticles in few to few tens of nm in the region, so the quantum confinement effect doesn't work significantly. Therefore, the trend in the optical gap energy of the nanoparticles is not always linearly proportional to the trend in crystallite size. Fourth, the interband transition of an electron within the nanoparticles is also strongly affected by the chemical nature and cation distribution of the nanoparticles. Unfortunately, here we can't explain in detail the cation distribution of the $Fe_3O_4$ nanoparticles due to a lack of evidence. Fifth, technically the broad size distribution of the nanoparticles might also influence the optical gap energy given by samples as explained by (Amirsalari & Shayesteh, 2015). Furthermore, the effect of the synthesis temperature on the optical gap energy of nanoparticles can be displayed by Fig. 11.

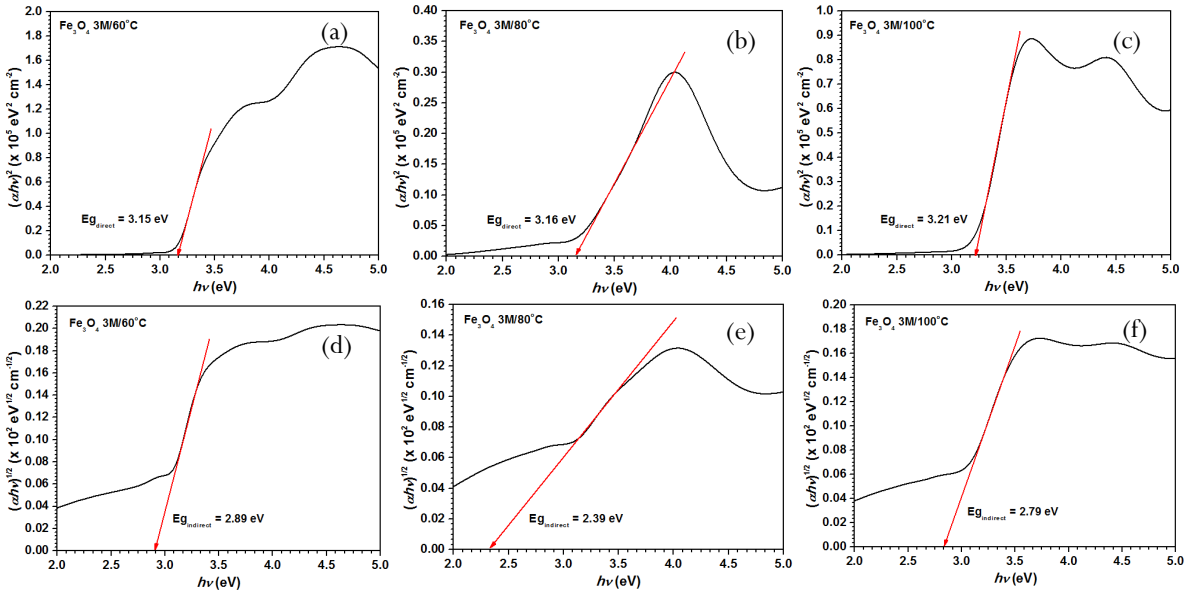


**Figure 11**. Tauch's plot for direct (a – c) and indirect (d – f) optical gap energies of $Fe_3O_4$ for synthesis temperature variation.

According to Fig. 11, the value of direct optical gap energy of the $Fe_3O_4$ nanoparticle increases with increasing synthesis temperature. On the other hand, the indirect optical gap energy of $Fe_3O_4$ nanoparticles has a decreasing value until the synthesis temperature of 80°C and back to increase at a temperature of 100°C. The value at which synthesis temperature equals to 80°C becomes a critical point of the indirect gap energy. An increase in optical bandgap might be caused by the defect levels occur in the valence band and conduction band with increasing synthesis temperature. However, the synthesis temperature also directly affects the crystallite size of nanoparticles and their distribution. A unique phenomenon also occurs in this finding at which an increase of crystallite size due to an increase of synthesis temperature followed by an increase of direct optical gap energy. An increase of optical gap energy, in this case, might be caused by the presence of intragap states between the valence band and conduction band due to temperature. Other reasons are the same as the case at which NaOH concentration is varied.

In general, this research found that the values of direct optical gap energy of nanoparticle are in the range of 3.15 eV – 3.39 eV. These values are much larger compared to the result reported by (Abd, et al., 2016). The indirect optical gap energy has value in the range of 2.39 eV – 2.91 eV. The direct optical gap energy is larger than the indirect optical gap energy due to the characteristic of nanoparticle crystalline in nature (Dhineshbabu, et

al., 2016). Other reasons can be addressed to the nature of Tauch's equation (3) for finding the value of optical gap energy as explained in detail by (Indrayana, et al., 2019). Finally, the trend of the optical gap energy ascribed that the $Fe_3O_4$ nanoparticle is semiconductor in nature.

## CONCLUSIONS AND SUGGESTIONS

The $Fe_3O_4$ nanoparticles with NaOH concentration and synthesis temperature variation have been successfully synthesized. The nanoparticles contain single phase structure i.e. spinel $Fe_3O_4$. The microstructural and optical properties of nanoparticles are strongly correlated to the NaOH concentration and synthesis temperature. Higher NaOH concentration and synthesis temperature results in larger particle size. NaOH concentration and synthesis temperature also affect defect levels within the unit cell. Both particle size and defect strongly influence the optical properties of the $Fe_3O_4$ nanoparticles. The $Fe_3O_4$ nanoparticle is a semiconductor in nature so that it can be a potential candidate for nano-electronics and photonic materials for many fields of application.

We suggest that further research has to do a more comprehensive measurement of the cation distribution of sample nanoparticles by using appropriate techniques such as Mössbauer Spectroscopy and X-Ray Absorption Spectroscopy. Knowing the cation distribution and the local structure of the nanoparticle will allow us to get more evidence empirically to justify the optical properties of nanoparticle.

## AKNOWLEDGEMENTS

The authors would like thank to the Government of Indonesia for the financial support for this research toward PDP Research Grant year 2018-2019 with a contract number of 118/SP2H/LT/DRPM/2019. We also would like thank to Universitas Halmahera throughout LPPMP for facilitating the administration.

## REFERENCES

Abd, A. N., Latif, D. M. A. & Abdulridha, W. M., 2016. Synthesis and Some Physical Properties of Magnetite ($Fe_3O_4$) NPs. *Journal of Multidisciplinary Engineering Science Studies,* 2(3), pp. 341-345.

Ali, A. et al., 2013. *Potentiometric Urea Biosensor Utilizing Nanobiocomposite of Chitosan-Iron Oxide Magnetic Nanoparticles.* Calgary Canada, IOP Publishing, pp. 1-11.

Ali, A. et al., 2016. Synthesis, Characterization, Applications, and Challenges of Iron Oxide Nanoparticles. *Nanotechnology, Science and Applications,* Volume 9, pp. 49-67.

Amirsalari, A. & Shayesteh, S. F., 2015. Effects of pH and Calcination Temperature on Structural and Optical Properties of Alumina Nanoparticles. *Superlattices and Microstructures,* Volume 82, p. 507–524.

Anjum, S., Fayyaz, J., Khurram, R. & Zia, R., 2018. Tuning of Magnetic and Optical Properties of $Co_{0.8}Zn_{0.2}Fe_2O_4$ Spinel Ferrite Thin Films Based on Post Annealing Temperature. *Journal of Superconductivity and Novel Magnetism,* pp. 1-12.

Anush, S. M. & Vishalakshi, B., 2019. Modified Chitosan Gel Incorporated with Magnetic Nanoparticle for Removal of Cu(II) and Cr(VI) from Aqueous Solution. *International Journal of Biological Macromolecules,* Volume 133, pp. 1051-1062.

Dhas, C. R. et al., 2015. Visible Light Driven Photocatalytic Degradation of Rhodamine B and Direct Red Using Cobalt Oxide Nanoparticles. *Ceramics International,* Volume 41, p. 9301–9313.

Dhineshbabu, N. R., Rajendran, V., Nithyavathy, N. & Vetumperumal, R., 2016. Study of Structural and Optical Properties of Cupric Oxide Nanoparticles. *Applied Nanoscience,* Volume 6, p. 933–939.

Faraji, M., Yamini, Y. & Rezaee, M., 2010. Magnetic Nanoparticles: Synthesis, Stabilization, Functionalization, Characterization, and Application. *Journal of the Iranian Chemical Society,* 7(1), pp. 1-37.

Ghandoor, H. E., Zidan, H. M., Khalil, M. M. H. & Ismail, M. I. M., 2012. Synthesis and Some Physical Properties of Magnetite ($Fe_3O_4$) Nanoparticles. *International Journal of Electrochemical Science,* Volume 7, pp. 5734 - 5745.

Ghazanfari, M. R., Kashefi, M., Shams, S. F. & Jaafari, M. R., 2016. Perspective of $Fe_3O_4$ Nanoparticles Role in Biomedical Applications. *Biochemistry Research Internation,* Issue 7840161, pp. 1-32.

Hameed, A., Mushtaq, H. M. & Hussain, M., 2017. Magnetite ($Fe_3O_4$) - Synthesis, Functionalization and its Application. *International Journal of Food and Allied Sciences,* 3(2), pp. 64-75.

Heiba, Z. K., Mohamed, M. B. & Imam, N. G., 2015. Structural Tuning of CdS Nanoparticles with Nucleation Temperature and Its reflection on the Optical Properties.

*Journal of Molecular Structure,* Volume 1094 , p. 91–97.

Hu, P. et al., 2019. Temperature Effects on Magnetic Properties of $Fe_3O_4$ Nanoparticles Synthesized by the Sol-Gel Explosion-Assisted Method. *Journal of Alloys and Compounds,* Volume 773, pp. 605-611.

Indrayana, I. P. T., Tjuana, L. A., Tuny, M. T. & K., 2019. *Nanostructure and Optical Properties of $Fe_3O_4$: Effect of Calcination Temperature and Dwelling Time.* Makassar, IOP Publishing, pp. 1-8.

Loganathan, A. & Kumar, K., 2016. Effects on Structural, Optical, and Magnetic Properties of Pure and Sr-Substituted $MgFe_2O_4$ Nanoparticles at Different Calcination Temperatures. *Applied Nanoscience,* Volume 6, p. 629–639.

Lopez, J. A. et al., 2010. Synthesis and Characterization of $Fe_3O_4$ Magnetic Nanofluid. *Revista Latinoamericana de Metalurgia y Materiales,* 30(1), pp. 60-66.

Mahdavi, M. et al., 2013. Synthesis, Surface Modification and Characterisation of Biocompatible Magnetic Iron Oxide Nanoparticles for Biomedical Applications. *Molecules,* Volume 18, pp. 7533-7548.

Mascolo, M. C., Pei, Y. & Ring, T. A., 2013. Room Temperature Co-Precipitation Synthesis of Magnetite Nanoparticles in a Large pH Window with Different Bases. *Materials,* Volume 6, pp. 5549-5567.

Mathew, D. S. & Juang, R. S., 2007. An Overview of the Structure and Magnetism of Spinel Ferrite Nanoparticles and Their Synthesis in Microemulsions. *Chemical Engineering Journal,* Volume 129, pp. 51-65.

Mohammad, L., Gomma, H. G., Ragab, D. & Zhu, J., 2017. Magnetic Nanoparticles for Environmental and Biomedical Applications: A Review. *Particuology,* Volume 30, pp. 1-14.

Mote, V. D., Dargad, J. S., Purushotham, Y. & Dole, B. N., 2015. Effect of Doping on Structural, Physical, Morphological and Optical Properties of $Zn_{1-x}Mn_xO$ Nanoparticles. *Ceramics International,* Volume 41, p. 15153–15161.

Murgueitio, E. et al., 2018. Green Synthesis of Iron Nanoparticles: Application on the Removal of Petroleum Oil from Contaminated Water and Soils. *Journal of Nanotechnology,* pp. 1-8.

Qu, J., Dong, Y., Wang, Y. & Xing, H., 2015. A Novel Sensor Based on $Fe_3O_4$ Nanoparticles–Multiwalled Carbon Nanotubes Composite Film for Determination of Nitrite. *Sensing and Bio-Sensing Research,* Volume 3, pp. 74-78.

Rahman, O. u., Mohapatra, S. C. & Ahmad, S., 2012. $Fe_3O_4$ Inverse Spinal Superparamagnetic Nanoparticles. *Materials Chemistry and Physics,* Volume 132, p. 196– 202.

Ramadan, W., Kareem, M., Hannoyer, B. & Saha, S., 2011. Effect of pH on the Structural and Magnetic Properties of Magnetite Nanoparticles Synthesized by Coprecipitation. *Advanced Materials Research,* Volume 324, pp. 129-132.

Raz, M. et al., 2012. Controlled Synthesis, Characterization and MagneticProperties of Magnetite ($Fe_3O_4$) Nanoparticles without Surfactant under N2 Gas at Room Temperature. *Key Engineering Materials,* Volume 492-493, pp. 746-751.

Reddy, H. K. & Yun, Y. S., 2016. Spinel Ferrite Magnetic Adsorbents: Alternative Future Materials for Water Purification?. *Coordination Chemistry Reviews,* Volume 315, pp. 90-111.

Revia, R. A. & Zhang, M., 2016. Magnetite Nanoparticles for Cancer Diagnosis, Treatment, and Treatment Monitoring: Recent Advances. *Materials Today,* 19(3), pp. 157-168.

Salviano, L. B. et al., 2018. Microstructural Assessment of Magnetite Nanoparticles ($Fe_3O_4$) Obtained by Chemical Precipitation Under Different Synthesis Conditions. *Materials Research,* 21(2), pp. 1-7.

Saranya, T., Parasuraman, K., Anbarasu, M. & Balamurugan, K., 2015. XRD, FTIR and SEM Study of Magnetite ($Fe_3O_4$) Nanoparticles Prepared by Hydrothermal Method. *Nano Vision: An International Research Journal of Nano Science & Technology,* 5(6), pp. 149-154.

Scott , B. L., 2007. *Magneto-Optical Study of Cobalt Ferrite Nanoparticles,* new Orleans: University of New Orleans.

Siregar, N. et al., 2017. *Effect of Synthesis Temperature and NaOH Concentration on Microstructural and Magnetic Properties of $Mn_{0.5}Zn_{0.5}Fe_2O_4$ Nanoparticles.* Malang, IOP Publishing, pp. 1-9.

Tai, M. F. et al., 2014. Facile Synthesis of Magnetite Iron Oxide Nanoparticles via Precipitation Method at Different Reaction Temperatures. *Materials Research Innovations,* 18(6), pp. 470-473.

Takai, Z. I., Mustafa, M. K., Asman, S. & Sekak, K. A., 2019. Preparation and Characterization of Magnetite ($Fe_3O_4$) Nanoparticles By Sol-

Gel Method. *International Journal of Nanoelectronics and Materials,* 12(1), pp. 37-46.

Tiley, R. J. D., 2011. *Colour and the Optical Properties of Materials: An Exploration of the Relationship Between Light, the Optical Properties of Materials and Colour.* United Kingdom: John Wiley & Sons, Ltd.

Yusoff, A., Salimi, M. N. & Jamlos, M. F., 2017. *Synthesis and Characterization of Biocompatible $Fe_3O_4$ Nanoparticles at Different pH.* s.l., AIP Publishing, pp. 1-4.